The Astrophysical Journal, 694:L59–L63, 2009 March 20 doi:10.1088/0004-637X/694/1/L59

MILLIMETER DETECTION OF AlO (X $^2\Sigma^+$): METAL OXIDE CHEMISTRY IN THE ENVELOPE OF VY CANIS MAJORIS

E. D. Tenenbaum and L. M. Ziurys
Department of Astronomy, Department of Chemistry, Steward Observatory, and Arizona Radio Observatory, University of Arizona, 933 N. Cherry Avenue, Tucson, AZ 85721, USA; emilyt@as.arizona.edu, lziurys@as.arizona.edu
Received 2008 December 7; accepted 2009 February 4; published 2009 February 27

ABSTRACT

A new circumstellar molecule, the radical AlO (X $^2\Sigma^+$), has been detected toward the envelope of the oxygen-rich supergiant star VY Canis Majoris (VY CMa) using the Arizona Radio Observatory (ARO). The $N = 7 \rightarrow 6$ and $6 \rightarrow 5$ rotational transitions of AlO at 268 and 230 GHz were observed at 1 mm using the ARO Submillimeter Telescope (SMT) and the $N = 4 \rightarrow 3$ line was detected at 2 mm using the ARO 12 m telescope. Based on the shape of the line profiles, AlO most likely arises from the dust-forming region in the spherical outflow of VY CMa, as opposed to the blue or redshifted winds, with a source size of $\theta_s \sim 0\farcs5$. Given this source size, the column density of AlO was found to be $N_{tot} \sim 2 \times 10^{15}$ cm^{-2} for $T_{rot} \sim 230$ K, with a fractional abundance, relative to H_2, of $\sim 10^{-8}$. Gas-phase thermodynamic equilibrium chemistry is the likely formation mechanism for AlO in VY CMa, but either shocks disrupt the condensation process into Al_2O_3, or chemical "freezeout" occurs. The species therefore survives further into the circumstellar envelope to a radius of $r \sim 20\ R_*$. The detection of AlO in VY CMa is additional evidence of an active gas-phase refractory chemistry in oxygen-rich envelopes, and suggests such objects may be fruitful sources for other new oxide identifications.

Key words: astrochemistry – circumstellar matter – ISM: molecules – radio lines: stars – stars: individual (VY CMa)

1. INTRODUCTION

Aluminum, the 12th most abundant element in space, is the most refractive of the 20 leading elements in the Periodic Table (Lodders 2003). This high degree of refractivity translates into substantial interstellar depletions of gas-phase aluminum; in diffuse clouds, for example, 90%–99% of this element is thought to be depleted into grains (Turner 1991a). Despite aluminum's propensity to condense, the element exhibits significant gas-phase chemistry in carbon-rich circumstellar environments. Toward the C-rich shell of the AGB star IRC +10216, millimeter spectra of AlCl, AlF, and AlNC have been detected, revealing an active synthesis involving aluminum in both the inner and outer regions of the envelope (Cernicharo & Guélin 1987; Ziurys et al. 1994, 2002). In addition, AlF has also been observed in the C-rich protoplanetary nebula CRL 2688 (Highberger et al. 2001).

In oxygen-rich envelopes, on the other hand, there has been little evidence of circumstellar gas-phase aluminum chemistry. Photospheric electronic transitions of AlO have been observed in a number of O-rich giant stars, including peculiar objects such as V4332 Sgr (Banerjee et al. 2003) as well as lines of TiO, ScO, and VO (e.g., Barnbaum et al. 1996; Tylenda et al. 2005). Turner (1995) predicted that the chemistry of this element in O-rich shells should mimic that in C-rich envelopes, and species such as AlF and AlCl should be observable in these objects. However, millimeter searches for aluminum-containing molecules in O-rich circumstellar gas have been unsuccessful (e.g., Turner 1991a, 1995), suggesting that the chemistry in O-rich shells is not particularly active, with few exotic refractory species (Olofsson 1997).

Recent studies of the red supergiant star VY Canis Majoris (VY CMa), however, have made evident the need to revisit refractory chemistry in O-rich envelopes. In the circumstellar shell of this massive star, NaCl, PN, and PO have been recently identified (Milam et al. 2007, 2008; Tenenbaum et al. 2007). While NaCl and PN are molecules observed in other C-rich circumstellar shells, PO is a completely new interstellar molecule. These results suggest that VY CMa and similar objects may be ideal candidates for identification of other refractory species, in particular oxides. Churchwell et al. (1980) did conduct a search for TiO in circumstellar gas using the NRAO 36 ft dish, including VY CMa, but the species was not identified with limits of ~0.2–0.5 K. This sensitivity can be vastly improved with the advances in millimeter technology since 1980.

Here we report the detection of AlO in the circumstellar shell of VY CMa. This molecule was identified on the basis of three rotational transitions observed in the 2 and 1 mm atmospheric windows. The identification was in part made possible because of new mixer technology developed for the Atacama Large Millimeter Array (ALMA); see Lauria et al. (2006). In this Letter, we report our measurements, derive an abundance and distribution for AlO in VY CMa, and discuss implications for aluminum chemistry in O-rich circumstellar shells.

2. OBSERVATIONS

The measurements were conducted between 2008 April and 2008 November using the Arizona Radio Observatory's (ARO) 10 m Submillimeter Telescope (SMT) on Mt. Graham for the 1 mm observations, and 12 m telescope on Kitt Peak for the 2 mm work. Both telescopes were operated in a beam-switching mode with a $\pm 2'$ subreflector throw. Pointing and focusing were conducted every 1–2 hr using observations of Mars or Saturn, and local oscillator shifts were done to check for image contamination. Observing frequencies, beam sizes, and efficiencies are listed in Table 1. The position used for VY CMa was $\alpha = 07^h20^m54\fs7$ $\delta = -25^\circ40'12''$ (B1950.0). Spectra were averaged weighted by the inverse square of the system temperature, and linear baselines were removed.

Table 1
Line Parameters of Observed AlO Transitions[a]

Transition	Frequency[b] (MHz)	η^c	θ_b ($''$)	V_{LSR} (km s^{-1})	T_A^* (K)	$\Delta V_{1/2}$ (km s^{-1})	$\int T_A^* dV$ (K km s^{-1})
$N = 7 \rightarrow 6$	267,937	0.78	28	25 ± 5	0.007 ± 0.002	63 ± 10	0.36 ± 0.09
$N = 6 \rightarrow 5$	229,670	0.78	33	25 ± 6	0.003 ± 0.001	55 ± 10	0.20 ± 0.05
$N = 4 \rightarrow 3$	153,124	0.74	41	27 ± 6	0.0014 ± 0.0005[d]	29 ± 4	0.05 ± 0.01[d]

Notes.
[a] Quoted errors are 3σ.
[b] Center of hyperfine pattern.
[c] η_b for SMT data, η_c for 12 m data (see text).
[d] Converted from T_R^* to T_A^* using $\eta_{fss} = 0.68$ (see text).

At the SMT, the 1 mm observations were conducted using a dual-channel, sideband-separating receiver featuring mixers developed for ALMA Band 6 (211–275 GHz). System temperatures ranged from 190 K to 450 K, and image rejection was consistently >15 dB. The backend used was a 1 MHz resolution filter bank with 2048 channels configured in a parallel mode (2 × 1024 channels). The SMT temperature scale is given in terms of T_A^*, which is the chopper-wheel-corrected antenna temperature (see Davis & vanden Bout 1973). The radiation temperature T_R is then defined as $T_R = T_A^*/\eta_b$, where η_b is the main-beam efficiency.

The 2 mm observations at the 12 m telescope utilized a dual-channel, cooled SIS mixer operated in a single sideband mode with typical image rejection >20 dB. System temperatures on the sky were ~200–500 K. Filter banks of 1 and 2 MHz resolution were employed simultaneously, with each bank composed of 256 channels configured in a parallel mode (2 × 128 channels). The temperature scale, given in T_R^*, is the chopper wheel antenna temperature corrected for forward spillover losses. In this case, $T_R = T_R^*/\eta_c$, where η_c is the corrected beam efficiency. For consistency, the 12 m results have been converted to the T_A^* scale using the relationship $T_A^* = T_R^* \times \eta_{fss}$, where η_{fss} is the forward spillover efficiency (see Kutner & Ulich 1981), and $\eta_b = \eta_{fss} \times \eta_c$ ($\eta_{fss} = 0.68$ for the 12 m telescope).

3. RESULTS

Three rotational transitions of AlO were detected: the $N = 7 \rightarrow 6$ and $6 \rightarrow 5$ lines at 268 and 230 GHz, as well as the $N = 4 \rightarrow 3$ transition near 153 GHz. These data are presented in Figure 1. AlO is a radical with a $^2\Sigma$ ground state, and the ^{27}Al nucleus has a spin of $I = 5/2$. The rotational levels of this species are therefore split by both fine and hyperfine interactions. The net result is that each rotational transition consists of 10–12 favorable, closely spaced hyperfine components, as shown under the spectra displayed in Figure 1. Several of the components are virtually coincident in frequency and therefore certain marker lines represent the sum of several features. For the $N = 7 \rightarrow 6$ and $N = 6 \rightarrow 5$ transitions, the hyperfine components are sufficiently close in frequency that they cannot be resolved in the detected AlO features, which have $\Delta V_{1/2} \sim 55$–63 km s^{-1}. It should be noted that typical line widths (FWHM) of molecules in VY CMa fall in the range of 40–70 km s^{-1}, depending on the number of kinematic components present (see Ziurys et al. 2007, 2009). In the $N = 4 \rightarrow 3$ transition, the favorable hyperfine components are more spread out in frequency than the 1 mm transitions, diluting the signal strength. The apparent line width of this transition is $\Delta V_{1/2} \sim 30$ km s^{-1}, which reflects the positions of the two strongest blends of hyperfine components (see Figure 1). The center of all the lines corresponds to a LSR velocity of $V_{LSR} \sim 25$ km s^{-1}, as found for other species in this source (e.g., Kemper et al. 2003; Ziurys et al. 2009). The intensities of the AlO features decrease from 7 to 3 to 1 mK (T_A^*), from higher to lower frequency, consistent with the increased beam size and hyperfine dilution. Measured line parameters are given in Table 1.

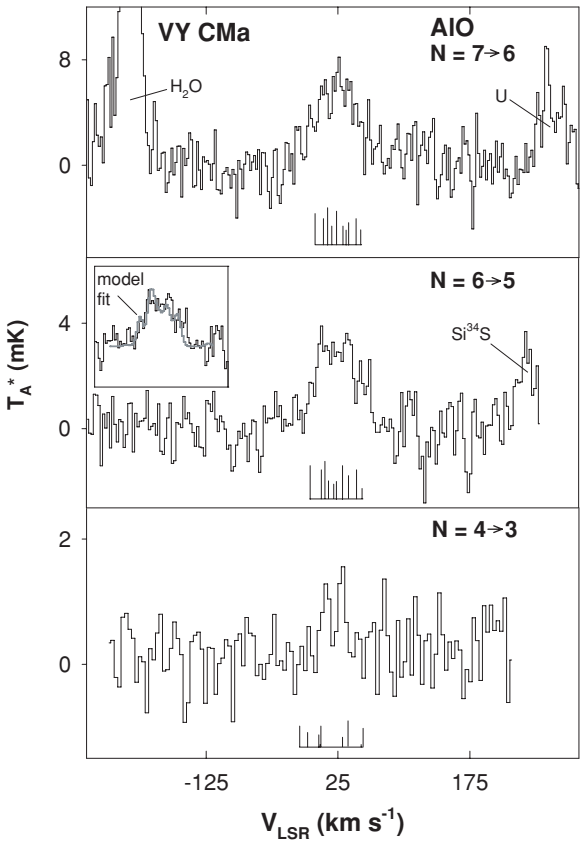

Figure 1. Spectra of the $N = 7 \rightarrow 6$ and $6 \rightarrow 5$ transitions of AlO ($X\ ^2\Sigma^+$) observed with the ARO SMT at 1 mm, as well as the $N = 4 \rightarrow 3$ line of this molecule measured at 2 mm with the ARO 12 m telescope. Positions and relative intensities of the individual hyperfine components of AlO are marked under the spectra, assuming $V_{LSR} = 25$ km s^{-1}. Spectral resolution for all data is 2 MHz, corresponding to 2.2 km s^{-1}, 2.6 km s^{-1}, and 3.9 km s^{-1} for the $N = 7 \rightarrow 6$, $6 \rightarrow 5$, and $4 \rightarrow 3$ lines, respectively. The intensity scale of the 12 m data ($N = 4 \rightarrow 3$) has been converted from T_R^* to T_A^*. The profiles vary between the three transitions, reflecting in part the different frequency splittings of the hyperfine components. An inset is shown for the middle panel, which displays the modeled line profile (in gray) for a line width of 10 km s^{-1} (see text). The feature labeled "U" is unidentified.

The spectroscopic literature was searched to assess the possibility of contamination of the AlO transitions by other spectral features. With one unlikely exception, there are no other plausible lines that can account for the observed emission.

Exactly coincident with the $N = 6 \rightarrow 5$ line of AlO are the spin-rotation doublets of the $N = 26 \rightarrow 25$ transition of $Ca^{37}Cl$ at 229,657 MHz and 229,698 MHz, respectively. Not only has CaCl never been detected, but our observations of the $Ca^{35}Cl$ lines at 236.5 GHz give an upper limit to the intensity of 3 mK. This sensitivity translates to a 1 mK upper limit for the $Ca^{37}Cl$ contaminating doublet, which is significantly less than the observed ~7 mK line of the AlO feature. It should be noted that the frequencies of the AlO, $N = 7 \rightarrow 6$ hyperfine transitions were directly measured by Yamada et al. (1990). The $N = 6 \rightarrow 5$ and $N = 4 \rightarrow 3$ frequencies, however, were predicted from these authors' spectroscopic constants. Based on comparison with the measured transitions, we estimate the uncertainties of the $N = 6 \rightarrow 5$ and $N = 4 \rightarrow 3$ line positions to be less than ± 1 MHz.

4. DISCUSSION

4.1 Abundance and Origin of AlO in the Circumstellar Flow

In the mm/submm wave spectrum of VY CMa, molecular line profiles vary widely between species. The variation is due to the presence of three distinct kinematic outflows: a redshifted component occurring at $V_{LSR} \sim 42$ km s^{-1}, a blueshifted wind near $V_{LSR} \sim -7$ km s^{-1}, and a spherical flow centered at $V_{LSR} \sim$ 20–25 km s^{-1} (Ziurys et al. 2007, 2009). Emission from some molecules such as SO_2 exclusively traces the red and blueshifted flows. Other species, like CS, show emission from all three components (see Ziurys et al. 2009). Some molecules appear to only emit from the central outflow, as is the case for PN. The central flow has a typical line width (FWHM) of ~30–35 km s^{-1}, and FWZP near 60 km s^{-1}, reflecting the terminal expansion velocity of $V_{exp} \sim 30$ km s^{-1} (e.g., Richards et al. 1998). For NaCl, however, the LSR velocity is indicative of the spherical flow but the FWHM line widths are much narrower: 15–16 km s^{-1}. These line widths suggest that NaCl arises from a region closer to the star where the gas has not reached its full expansion velocity and dust is still forming (Milam et al. 2007).

In the case of AlO, the hyperfine structure complicates the interpretation of the kinematics. Nevertheless, the $N = 4 \rightarrow 3$ transition suggests that the individual line widths of the hyperfine components are narrow, typically 10–15 km s^{-1}, as seen in NaCl. By modeling the AlO profiles with a 10 km s^{-1} line width and assuming the species arises from the spherical flow, the spectral profiles can be reproduced reasonably well, given the signal-to-noise ratio, as shown in the inset in Figure 1. These simulations were carried out by creating an emission-line profile for every AlO hyperfine component, with the intensity adjusted for relative transition strength, and then summing over the individual intensities. Modeling with red and blueshifted outflows, with or without the central component, did not successfully reproduce the profiles, ruling out these winds as sources of AlO emission.

The expansion velocity profile of the circumstellar shell of VY CMa is not well known. However, water maser observations of Richards et al. (1998) suggest that the terminal velocity is achieved near a radius of $r \approx 0\farcs5$ or 8.5×10^{15} cm, corresponding to ~40 R_* ($R_* = 2 \times 10^{14}$ cm; Monnier et al. 2000). Based on the modeling, AlO appears to be present in gas that is still accelerating with $r < 0\farcs5$. Modeling the line profiles for NaCl indicated a source radius of $0\farcs25$ (Milam et al. 2007). Assuming that AlO arises from a similar region with $r \sim 0\farcs25$ (~20 R_*), then the column density of this molecule is $N_{tot} \sim 2 \times 10^{15}$ cm^{-2}, and $T_{rot} \sim 230$ K, using the rotational diagram method (Turner 1991b). The $0\farcs5$ source size is consistent with the relative intensities of the three transitions. Moreover, the rotational temperature of $T_{rot} \sim 230$ K reflects the high gas kinetic temperature at this radius. The column density was derived using the following equation, which assumes optically thin emission and LTE excitation:

$$\ln\left[\frac{3k\int(T_R dv)}{8\pi^3 g_J \nu |\mu_{ul}|^2}\right] = \ln\left[\frac{N_{tot}}{Q_{rot}}\right] - \frac{E_u}{T_{rot}}. \quad (1)$$

Here $\int(T_R dv)$ is the efficiency-corrected line integral, g_J is the rotational degeneracy of the upper level, and E_u is the energy of the upper level, ν is the transition frequency, $|\mu_{ul}|^2$ is the dipole moment matrix element of the transition, and Q_{rot} is the rotational partition function. This method is appropriate for trace species such as AlO, especially since its collisional cross sections are unknown. Using a distance to VY CMa of 1.14 kpc (Choi et al. 2008), and a mass-loss rate of $2.6 \times 10^{-4}\ M_\odot$ yr^{-1} for the spherical flow (adjusted for updated distance, Humphreys et al. 2005; Monnier et al. 2000), the AlO fractional abundance relative to H_2 is $\sim 10^{-8}$—roughly two orders of magnitude less than the cosmic abundance of aluminum (Lodders 2003).

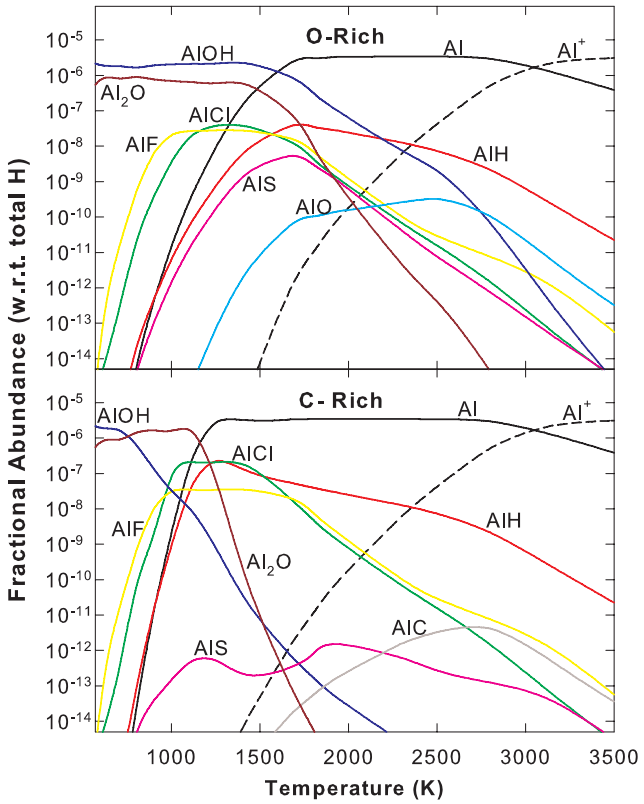

Figure 2. Results of model calculations of LTE abundances of aluminum-bearing molecules relative to total hydrogen ($H_2 + H + H^+$), plotted as a function of temperature. Calculations were done at $P_g = 3.0$ using the model of Tsuji (1973), modified with updated cosmic abundances from Lodders (2003). The upper panel data were calculated for the oxygen-rich situation with C/O ~ 0.5, and the lower panel data represent carbon-rich gas with C/O ~ 1.5.

4.2 Aluminum Chemistry in Oxygen-Rich Envelopes

Given the small spatial extent of AlO, it is reasonable to consider gas-phase thermodynamic equilibrium (LTE) chemistry as a formation mechanism. Results of LTE chemistry calculations in an O-rich envelope (C/O ~ 0.5), carried out with the model of Tsuji (1973) using updated cosmic abundances (Lodders 2003), are shown in the upper portion of Figure 2. AlO is predicted to

form close to the photosphere with an abundance of $f\left(\mathrm{AlO}/\mathrm{H_2}\right) \approx 6 \times 10^{-10}$ at $T \sim 2500$ K. (Note $\mathrm{H_2} \approx \mathrm{H_2} + \mathrm{H} + \mathrm{H^+}$.) By $T \sim 1200$ K ($\sim 4\ R_*$), the abundance rapidly drops to $f \sim 10^{-14}$ (see Figure 2). Beyond $T \sim 1500$ K, AlOH, and $\mathrm{Al_2O}$ become the major sinks of aluminum with $f\left(\mathrm{AlOH}/\mathrm{H_2}\right) \sim 5 \times 10^{-6}$ and $f\left(\mathrm{Al_2O}/\mathrm{H_2}\right) \sim 1 \times 10^{-6}$. This model therefore does not appear to reproduce the observed AlO abundance, nor its spatial extent. Furthermore, observations of the 1 mm AlOH transition frequencies show no emission from this molecule down to a 3σ noise level of 9 mK.

Since aluminum is highly refractory, grain condensation should also be considered. Of the dust types predicted to form in an O-rich circumstellar envelope, $\mathrm{Al_2O_3}$ (aka alumina), has the highest condensation temperature: $T_{\mathrm{cond}} \sim 1700$ K (Lodders 2003; Lodders & Fegley 1999). Thus, it is expected that alumina grains will form first as material flows from the star. In fact, over 130 crystalline and amorphous alumina presolar grains have been isolated from chondritic meteorites, showing isotopic signatures that indicate an origin in the outflows of O-rich RGB, AGB, and possibly supergiant stars (Nittler et al. 2008). Sharp & Hubner (1990) have constructed an astrophysical model combining LTE gas-phase and condensation chemistry, considering solar system elemental abundances (C/O ~ 0.5, i.e., O > C, as in VY CMa). Their calculations predict $f\left(\mathrm{AlO}/\mathrm{H_2}\right) \sim 10^{-8}$ near the photosphere at 1800 K ($2\ R_*$ for VY CMa), i.e. a higher abundance than the purely gas-phase LTE model by a factor of $\sim$20. An important aspect of the Sharp & Hubner (1990) model is that abundances of refractory-bearing molecules decrease closer to the star when condensation is considered. For example, the $\mathrm{Al_2O}$ abundance drops precipitously at temperatures below 1600 K.

While our observed aluminum monoxide abundance of $\sim 10^{-8}$ qualitatively agrees with the predictions of Sharp & Hubner (1990), our observations suggest a larger spatial extent than $\sim 2\ R_*$. One explanation for the more extended distribution of AlO is that shocks in the inner envelope are disrupting the condensation process, enabling the species to remain in the gas phase beyond its LTE-imposed boundary. Shock waves originating from large convective cells have been proposed as the origin of the erratic outflows in VY CMa (Ziurys et al. 2007). Moreover, calculations by Cherchneff (2006) show that shock effects can significantly alter LTE circumstellar chemistry near the stellar photosphere. An alternative explanation is that the abundances of AlO established at $2\ R_*$ from LTE chemistry are "frozen out". Chemical freezeout occurs because the temperature and density drop rapidly in the expanding outflow, sharply curtailing molecular reactions such that LTE abundances are not significantly altered (McCabe et al. 1979). Near $20\ R_*$, the chemical and/or condensation timescales have overtaken that of the shell expansion and AlO consequently disappears.

Optical and near-IR studies of electronic transitions of AlO have shown that this species is present in stellar photospheres (e.g., Keenan et al. 1969). Recent observations of the $A\,^2\Pi_i$–$X\,^2\Sigma^+$ and $B\,^2\Sigma^+$–$X\,^2\Sigma^+$ transitions toward the stars V4332 Sgr, IRAS 08182−6000 and U Equa have suggested that there may be a possible nonphotospheric source of AlO located in the cooler dust shell regions (e.g., Banerjee et al. 2003). Unfortunately, there are no published near-IR (1.5 μm) or optical (5000 Å) high-resolution measurements of the AlO *A*–*X* and *B*–*X* bands in VY CMa, to our knowledge. Observations of this object in these spectral regions could enable a connection to be drawn between photospheric and circumstellar LTE chemistry.

4.3 Comparison with Carbon-Rich Circumstellar Environments

To date, three aluminum-bearing molecules have been detected in carbon-rich circumstellar envelopes. The metal halides AlF and AlCl, and the metal isocyanide AlNC were all identified via their millimeter rotational transitions toward the well studied C-rich AGB star IRC +10216 (Cernicharo & Guélin 1987; Ziurys et al. 1994, 2002). In addition, AlF has been detected in CRL 2688 (Highberger et al. 2001). In IRC +10216, AlCl and AlF both appear to have inner envelope distributions with source sizes $\leqslant 5''$, based on both Plateau de Bure interferometer maps (Guélin et al. 1997), and the flat-topped line shapes observed at the IRAM 30 m telescope (Cernicharo & Guélin 1987). In contrast, the clearly U-shaped line profiles of AlNC, observed with the 30 m antenna as well, indicate a shell distribution peaking at a radius of $10''$ (Ziurys et al. 2002). The inner envelope location of AlCl and AlF is a signature of formation by LTE chemistry near the photosphere, as predicted by the C-rich gas-phase model shown in the lower half of Figure 2. Conversely, the shell distribution of AlNC suggests synthesis via ion–neutral, neutral–neutral, or shock-induced reactions. One possible formation scenario is that the aluminum halides react with HCN farther out in the shell, and a ligand exchange reaction occurs (Petrie 1997).

When considering fractional abundances, AlCl and AlF contain $\sim$5% of aluminum in IRC +10216, with AlNC serving as a minor carrier, assuming the aluminum abundance is approximately equal to the cosmic value of $\mathrm{Al/H} \sim 3 \times 10^{-6}$ (Lodders 2003). In VY CMa, only $\sim$0.2% of aluminum is in the form of AlO. Based on these percentages, there appears to be less aluminum in gas-phase molecules in the O-rich envelope of VY CMa than in the C-rich analog, IRC +10216. Although these relative values could change with future observations, this difference may be due to condensation chemistry. The major Al-containing dust condensate in carbon-rich envelopes is predicted to be AlN, which forms at temperatures $\sim$300 K lower than its oxygen-rich counterpart, $\mathrm{Al_2O_3}$ (Lodders & Fegley 1999). Consequently, more aluminum may become locked in the solid phase in the inner envelope of an O-rich star than a C-rich one, limiting the formation of gas-phase Al-bearing molecules.

5. CONCLUSIONS

The detection of AlO in VY CMa is additional new evidence for an active gas-phase refractory chemistry in oxygen-rich circumstellar envelopes. Thus far, the refractory species detected in VY CMa (AlO, NaCl, PN, and PO) all appear to be confined to the inner region of the shell. In contrast, refractory species in IRC + 10216 have both inner (AlF, AlCl, NaCl, for example) and outer envelope distributions (AlNC, MgNC, MgCN), depending on the particular molecule. This result likely reflects differences in dust formation processes between these two types of objects. The detection of AlO is also of importance because it presents a future opportunity to probe the connection between the chemistry of the stellar photosphere and the inner circumstellar shell. Finally, this study suggests that additional new circumstellar molecules may be discovered in VY CMa and other O-rich envelopes.

We thank T. Tsuji, G. Herbig, and G. Wallerstein for their input to the Letter, and the ARO staff. This research is funded by NSF grant AST-0607803. E.D.T acknowledges financial support from the NSF Graduate Research Fellowship Program.

REFERENCES

Banerjee, D. P. K., Varricatt, W. P., Ashok, N. M., & Launila, O. 2003, ApJ, 598, L31
Barnbaum, C., Omont, A., & Morris, M. 1996, A&A, 310, 259
Cernicharo, J., & Guélin, M. 1987, A&A, 183, L10
Cherchneff, I. 2006, A&A, 456, 1001
Choi, Y. K., et al. 2008, PASJ, 60, 1007
Churchwell, E., Hocking, W. H., Merer, A. J., & Gerry, M. C. L. 1980, AJ, 85, 1382
Davis, J. H., & vanden Bout, P. 1973, ApL, 15, 43
Guélin, M., Lucas, R., & Neri, R. 1997, in CO: Twenty-Five Years of Millimeter-Wave Spectroscopy, ed. W. B. Latter et al. (Dordrecht: Kluwer), 359
Highberger, J. L., Savage, C., Bieging, J. H., & Ziurys, L. M. 2001, ApJ, 562, 790
Humphreys, R. M., Davidson, K., Ruch, G., & Wallerstein, G. 2005, AJ, 129, 492
Keenan, P. C., Deutsch, A. J., & Garrson, R. F. 1969, ApJ, 158, 261
Kemper, F., Stark, R., Justtanont, K., de Koter, A., Tielens, A. G. G. M., Waters, L. B. F. M., Cami, J., & Dijkstra, C. 2003, A&A, 407, 609
Kutner, M. L., & Ulich, B. L. 1981, ApJ, 250, 341
Lauria, E. F., Kerr, A. R., Reiland, G., Freund, R. F., Lichtenberger, A. W., Ziurys, L. M., Metcalf, M., & Forbes, D. 2006, ALMA Memo No. 553 (www.alma.nrao/memos)
Lodders, K. 2003, ApJ, 591, 1220
Lodders, K., & Fegley, B. Jr. 1999, in IAU Symp. 191, Asymptotic Giant Branch Stars, ed. T. Le Bertre, A. Lèbre, & C. Waelkens (San Francisco, CA: ASP), 279
McCabe, E. M., Connon Smith, R., & Clegg, R. E. S. 1979, Nature, 281, 263
Milam, S. N., Apponi, A. J., Woolf, N. J., & Ziurys, L. M. 2007, ApJ, 668, L131
Milam, S. N., Halfen, D. T., Tenenbaum, E. D., Apponi, A. J., Woolf, N. J., & Ziurys, L. M. 2008, ApJ, 684, 618
Monnier, J. D., Danchi, W. C., Hale, D. S., Lipman, E. A., Tuthill, P. G., & Townes, C. H. 2000, ApJ, 543, 861
Nittler, L. R., Alexander, C. M. O'D., Gallino, R., Hoppe, P., Nguyen, A. N., Stadermann, F. J., & Zinner, E. K. 2008, ApJ, 682, 1450
Olofsson, H. 1997, Ap&SS, 251, 31
Petrie, S. 1997, ApJ, 476, 191
Richards, A. M. S., Yates, J. A., & Cohen, R. J. 1998, MNRAS, 299, 319
Sharp, C. M., & Hubner, W. F. 1990, ApJS, 72, 417
Tenenbaum, E. D., Woolf, N. J., & Ziurys, L. M. 2007, ApJ, 666, L29
Tsuji, T. 1973, A&A, 23, 411
Turner, B. E. 1991a, ApJ, 376, 573
Turner, B. E. 1991b, ApJSS, 76, 617
Turner, B. E. 1995, Ap&SS, 224, 297
Tylenda, R., Crause, L. A., Górny, S. K., & Schmidt, M. R. 2005, A&A, 439, 651
Yamada, C., Cohen, E. A., Fujitake, M., & Hirota, E. 1990, J. Phys. Chem., 92, 2146
Ziurys, L. M., Apponi, A. J., & Phillips, T. G. 1994, ApJ, 433, 729
Ziurys, L. M., Savage, C., Highberger, J. L., Apponi, A. J., Guélin, M., & Cernicharo, J. 2002, ApJ, 564, L45
Ziurys, L. M., Milam, S. N., Apponi, A. J., & Woolf, N. J. 2007, Nature, 447, 1094
Ziurys, L. M., Tenenbaum, E. D., Pulliam, R. L., Woolf, N. J., & Milam, S. N. 2009, ApJ, in press